

FIG. 1. (a) Schematic workflow for VQNHE. The output state $|\psi\rangle = U(\boldsymbol{\theta})|0\rangle$ is attached with a small measurement circuit V . Measurement on computational (Z) basis is conducted on $VU(\boldsymbol{\theta})|0\rangle$ to collect shots of bitstring result as \vec{s} . With the zeroth qubit as the star qubit (see main text for details), $0s_{1:n-1}$ and $1\tilde{s}_{1:n-1}$ are fed into the classical neural network f with trainable weights ϕ . The expectation of \hat{H} can then be estimated according to Eq. (9). Finally parameters in both PQC and neural network are optimized with gradient based optimizer from the expectation result $\langle\hat{H}\rangle$. (b) Measurement protocol for $\hat{H} = Y_2Z_3X_4$. The star qubit corresponds to s_2 and CX gate is applied to qubit 4 since X_4 is in \hat{H} . Meanwhile, CZ gate is omitted in the hardware level and its effect is counted by the prefactor s_3 in the expression. (c) Measurement protocol for $\hat{H} = X_1X_2Y_3$. The star qubit corresponds to s_1 . CX and CY gates are applied on qubit 2 and 3 respectively, since there are X_2 and Y_3 in \hat{H} .

the quantum nature of the desired output is much harder to be embedded into a classical post-processing framework, very few works have explored this possibility. In Ref. [41], the authors applied the so-called Jastrow factor [42] $\hat{\mathcal{P}}(\phi) = \exp(\sum_{kl} \phi_{kl} Z_k Z_l)$ to the output state $|\psi_\theta\rangle$ of a quantum circuit, yielding the final target state $|\psi_f\rangle = \hat{\mathcal{P}}(\phi)|\psi_\theta\rangle$. However, existing proposals to supplement standard VQE with $\hat{\mathcal{P}}(\phi)$ suffer from two main drawbacks. Firstly, though the Jastrow factor is known for capturing quantum correlations in variational Monte Carlo (VMC) [43, 44], it is not the most general form of post-processing and thus the expressive power of such setup is quite limited. More importantly, $\hat{\mathcal{P}}(\phi)$ cannot be straightforwardly implemented on a quantum computer. Existing methods proposed to evaluate $\langle\psi_f|\hat{H}|\psi_f\rangle$ require an exponential amount of times or resources to achieve the same measurement accuracy as the standard VQE [41]. Specifically, in the entangled copies method, the probabilities of all bitstring measurements need to be reconstructed, which requires an exponential number of measurements. In the transformed Hamiltonian approach [45], the extra Jastrow operator is absorbed into the original Hamiltonian \hat{H} , and one needs to evaluate $\langle\psi|\hat{\mathcal{P}}\hat{H}\hat{\mathcal{P}}|\psi\rangle$. Since there is an exponential number of Pauli strings in the Taylor expansion of $\hat{\mathcal{P}}$, one has to evaluate exponential numbers of Pauli strings for the transformed Hamiltonian.

In this Letter, we introduce the variational quantum-neural hybrid eigensolver which falls into the paradigm of variational quantum algorithms enhanced by classical post-processing. Our approach successfully addresses both challenges encountered in the earlier attempts to

combine VQE with classical post-processing: (i) VQNHE possesses much greater expressive power as the post-processing can be modeled by any modern neural networks; (ii) VQNHE utilizes the same amount of quantum resource as the original VQE while the classical overhead is provably polynomial in the output range of the neural function and constant in terms of problem size. We emphasize that the rigorously proven polynomial efficiency of VQNHE is highly nontrivial as the nonunitary post-processing overhead in this scenario is often thought to be intrinsically exponential. Therefore, our approach presents the first scalable method to *exponentially* accelerate VQE with nonunitary post-processing.

Setup and Method: The schematic workflow of VQNHE is shown in Fig. 1(a). Suppose the output state from the PQC $U(\boldsymbol{\theta})$ is $|\psi\rangle = U(\boldsymbol{\theta})|0\rangle$. We propose the following nonunitary post-processing operator:

$$\hat{f} = \sum_{s \in \{0,1\}^n} f_\phi(s) |s\rangle \langle s|, \quad (1)$$

where $f_\phi(s)$ is a parameterized function of a bitstring s . Then the (unnormalized) target output state from VQNHE is $|\psi_f\rangle = \hat{f}|\psi\rangle$. The aim is to minimize the energy expectation

$$\langle\hat{H}\rangle_f = \frac{\langle\psi_f|\hat{H}|\psi_f\rangle}{\langle\psi_f|\psi_f\rangle} \quad (2)$$

by tuning variational parameters $\boldsymbol{\theta}$ in the PQC U and ϕ in the neural network f . When \hat{f} is applied to $|\psi\rangle$, it adjusts ψ_s , the quantum amplitude of $|\psi\rangle$ in the computational basis s . For the target ground state $|\psi_0\rangle$,

as long as $\{s : \psi_{0s} \neq 0\} \subseteq \{s : \psi_s \neq 0\}$, there always exists an \hat{f} such that $\hat{f}|\psi\rangle = |\psi_0\rangle$. In our setup, f_ϕ is implemented by a neural network with weights ϕ which can be learned in training. For example, Jastrow factor can be regarded as a special case of Eq. (1) as $f(s) = \exp(-\sum_{ij} \phi_{ij}(1-2s_i)(1-2s_j))$.

The key to enabling the above workflow is to efficiently evaluate Eq. (2). Since \hat{H} can be decomposed to a summation of Pauli strings, it suffices to compute the expectation for each Pauli string and then add them up. For this reason, we will assume without loss of generality that \hat{H} is a Pauli string in the following discussions. As we mentioned in the introduction, naïve implementations such as the transformed Hamiltonian approach generally lead to an exponential number of terms to measure which is not practical for any moderate-sized problem.

Firstly, the denominator of Eq. (2) is easy to estimate from measurements as

$$\langle \psi_f | \psi_f \rangle = \sum_{s \in \{0,1\}^n} |\psi_s|^2 |f(s)|^2. \quad (3)$$

The measurement protocol for Eq. (3) is straightforward: we simply measure the PQC U in computational (Z) basis for multiple shots for s , and compute the expectation of $|f(s)|^2$. If the Pauli string \hat{H} only contains I and Z operators, since $\langle s | \hat{H} | s' \rangle = H_s \delta_{ss'}$, the estimation for the numerator is also easy:

$$\langle \psi_f | \hat{H} | \psi_f \rangle = \sum_{s \in \{0,1\}^n} |\psi_s|^2 |f(s)|^2 H_s. \quad (4)$$

The key advantage of VQNHE is its efficient scheme to evaluate $\langle \psi_f | \hat{H} | \psi_f \rangle$ when \hat{H} contains X or Y operators. In this case, we label one of the qubits in the Pauli string with X or Y operator as the star qubit, and we rearrange the star qubit as the zero-th qubit in the derivation below. We further label $|\tilde{s}\rangle$ as the bitstring that satisfies $\hat{H}|s\rangle = S(\tilde{s})|\tilde{s}\rangle$, where $S = \pm 1, \pm i$ is the sign factor for such a basis transformation under \hat{H} . For example, for $\hat{H} = X_0 Y_1 Z_2$, $|011\rangle = |101\rangle$ and $S(101) = -i$. Since $\hat{H}^2 = 1$, all eigenvalues are ± 1 and $S(s)S(\tilde{s}) = 1$. The matrix form of \hat{H} can thus be expressed as

$$\hat{H} = \sum_{\substack{s_0=0, \\ s_{1:n-1} \in \{0,1\}^{n-1}}} S(s) |s\rangle \langle \tilde{s}| + S(\tilde{s}) |\tilde{s}\rangle \langle s|. \quad (5)$$

Note that the sum is over all bitstrings but with the star qubit fixed as $s_0 = 0$, and we use the shorthand notation $s \in 0s_{1:n-1}$ for simplicity. The 2^n eigenvectors of \hat{H} with eigenvalue ± 1 have simple forms $|\pm, s_{1:n-1}\rangle$:

$$|+, s_{1:n-1}\rangle = \frac{1}{\sqrt{2}} (S(0s_{1:n-1})|0s_{1:n-1}\rangle + |1\widetilde{s_{1:n-1}}\rangle) \quad (6)$$

$$|-, s_{1:n-1}\rangle = \frac{1}{\sqrt{2}} (S(0s_{1:n-1})|0s_{1:n-1}\rangle - |1\widetilde{s_{1:n-1}}\rangle). \quad (7)$$

We restrict f to real-valued functions for now; and for the general case of complex-valued post-processing f , efficient estimation is also possible (see the Supplemental Material for details). Then we obtain:

$$\begin{aligned} & \langle \psi_f | \hat{H} | \psi_f \rangle \\ &= \langle \psi | \left(\sum_{s \in 0s_{1:n-1}} f(s)f(\tilde{s})S(s)|s\rangle \langle \tilde{s}| + f(s)f(\tilde{s})S(\tilde{s})|\tilde{s}\rangle \langle s| \right) | \psi \rangle \\ &= \langle \psi | \left(\sum_{s \in 0s_{1:n-1}} f(s)f(\tilde{s})(|+, s\rangle \langle +, s| - |-, s\rangle \langle -, s|) \right) | \psi \rangle \\ &= \sum_{s \in 0s_{1:n-1}} |\psi_{+,s}|^2 f(s)f(\tilde{s}) + |\psi_{-,s}|^2 (-f(s)f(\tilde{s})), \quad (8) \end{aligned}$$

where $\psi_{\pm,s} = \langle \pm, s_{1:n-1} | \psi \rangle$.

To realize a measurement in the eigenbasis of \hat{H} , we attach a measurement circuit V after the original PQC $U(\theta)$ such that the computational basis measurement on the output from $VU(\theta)|0\rangle$ corresponds to the amplitude for $|\pm, s_{1:n-1}\rangle$, where the readout for first (star) qubit represents the eigenvalue of \hat{H} and the readout for the remaining $n-1$ qubits stand for $s_{1:n-1}$. Specifically, we require $V^\dagger|s\rangle \propto |\pm, s_{1:n-1}\rangle$ so that $\psi_{\pm,s} = \langle \pm, s_{1:n-1} | \psi \rangle = \langle s | VU(\theta) | 0 \rangle$. The problem is now reduced to efficiently building a measurement circuit V which gives $V^\dagger|s\rangle \propto (|0s_{1:n-1}\rangle + (1-2s_0)\hat{H}|0s_{1:n-1}\rangle)$. We now describe how to build this V circuit:

1. For all qubits present in the Pauli string \hat{H} except the star qubit, we apply a control-X/Y/Z gate with the control being the star qubit, and the choice of the control gate is determined by the Pauli operator acting on the corresponding qubit in \hat{H} . (Note that control-Z gate application can be omitted and replaced by counting the extra sign s_i in the final expression.)
2. The star qubit is measured in the X or Y basis determined by the corresponding operator in \hat{H} , or equivalently speaking, the star qubit is attached with a single-qubit gate: Hadamard gate in X case, and $R_x = \exp(-\pi/4 iX)$ rotation gate in Y case, and then measured on the computational (Z) basis.

We explicitly constructed the measurement circuit V for a few representative Pauli string \hat{H} , as shown in Fig. 1(b) and (c). By appending the aforementioned compact measurement circuit V to $U(\theta)$ and collecting measurement results as bitstring s , the expectation value from the quantum-neural hybrid state is given by:

$$\langle \hat{H} \rangle_{\psi_f} = \frac{\langle (1-2s_0)f(0s_{1:n-1})f(1\widetilde{s_{1:n-1}}) \rangle_{UV}}{\langle f(s)^2 \rangle_U}, \quad (9)$$

where bitstring s in the denominator is drawn from the PQC U and bitstring s in the numerator is drawn from the PQC with the measurement circuit V appended.

Model	TFIM	Heisenberg Model
VQE	-14.914 ($3 * 10^{-2}$)	-21.393 ($7 * 10^{-3}$)
VQNHE	-15.319 ($2 * 10^{-4}$)	-21.546 ($2 * 10^{-4}$)
exact	-15.3226	-21.5496

TABLE I. The ground state energies obtained from both VQE and VQNHE with the same PQC structure. for 1D TFIM and Heisenberg model with $N = 12$ sites. Relative errors compared to the exact ground state are included. For both models, the energy obtained from VQNHE is much closer to the exact ground state energy than the one obtained from VQE

The extra quantum resources compared to the original PQC for VQE is at most $m - 1$ two-qubit gates, where m is the number of X and Y operators in the Pauli string \hat{H} . For typical short-range interaction Hamiltonians, we note that $m = O(1)$. Besides, the number of measurement shots required to achieve the same accuracy as VQE is polynomial bounded in the VQNHE setup (see the Supplemental Materials for details of a rigorous proof). Now that we can efficiently evaluate $\langle \hat{H} \rangle_{\psi_f}$, the gradients with respect to the PQC and the neural network can be efficiently obtained via parameter shift [46–48] and back-propagation, respectively, which facilitate gradient-based classical optimizers to update parameters θ and ϕ .

With the presented formalism and protocol, we have demonstrated that VQNHE, the combination of variational quantum eigensolver and classical nonunitary neural post-processing, gives rise to an *exponential* acceleration compared to previous methods when incorporating non-unitary post-processing into the standard VQE.

Results: In this section, we report the performance of VQNHE on several benchmarks in modeling quantum spins and molecules, including 1D transverse field Ising model (TFIM), 1D Heisenberg model, LiH, H_6 -hexagon and H_6 -chain molecule [49]. (See the Supplemental Material for details on the setup and results for each system.)

First, we present numerical results for quantum spin models: the TFIM defined as $H_{\text{TFIM}} = \sum_{i,i+1} Z_i Z_{i+1} - \sum_i X_i$, and the Heisenberg model defined as $H_{\text{Heisenberg}} = \sum_{i,i+1} (X_i X_{i+1} + Y_i Y_{i+1} + Z_i Z_{i+1})$, both imposed with the periodic boundary condition. We apply both VQNHE and VQE to simulate the ground state of these systems with $N = 12$ sites. The results for the ground-state energy of these two systems are summarized in Table. I. Note that VQNHE provides a substantially more accurate estimation (about two orders of magnitude improvement in terms of energy estimation accuracy) of the ground-state energy using the same amount of quantum resources.

We further obtain the optimized energies from the VQE and VQNHE algorithms simulated on IBM quantum hardware and noisy simulators, as shown in Fig. 2. The target model is the 5-site TFIM model with open boundary condition. The results demonstrate that the

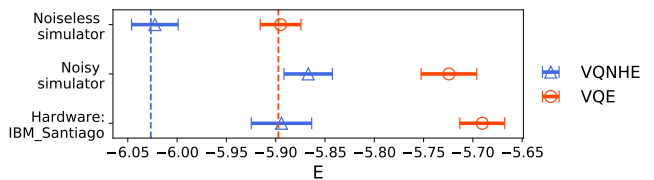


FIG. 2. Optimized energies on the 5-site TFIM model with open boundary condition using either VQNHE (blue) and VQE (red) approaches. Measurement-based results in noiseless, noisy simulators, and real quantum hardware are shown with the error bar. The vertical red and blue lines are the ideal optimized energy values from VQNHE and VQE, when no quantum noise or measurement uncertainty exists. The blue line also coincides with the exact ground state energy for the model since the ideal VQNHE result only has a relative error in the order of 10^{-12} .

VQNHE works well in the presence of quantum noise and measurement uncertainty on the real quantum hardware, namely, VQNHE exhibits a strong noise resilience because of the further optimization done with the post-processing module.

We now turn to the calculation of the energy dissociation curve for LiH, another common benchmark for VQE. The task is to calculate the ground-state energy of LiH at different bond distances. To obtain the Hamiltonian of LiH in terms of qubit operators, we firstly preprocess LiH using procedures including overlap integral calculation and qubit encoding for a fermionic Hamiltonian. These procedures are done using Psi4 [50] and OpenFermion [51], respectively. By using symmetry enforced binary code [52] on the complete active space of Hartree-Fock molecular orbitals, we obtain a 4-qubit Hamiltonian composed of 100 Pauli string terms.

We optimize LiH qubit Hamiltonian using VQNHE and VQE with 20 independent runs for each bond distance from 0.5 to 2.8Å, and the best results of each instance are reported in Fig. 3. Both VQNHE and VQE utilize the same depth-2 hardware efficient ansatz. The relative error of the VQNHE result is in the order of 10^{-5} and this result matches the state-of-the-art result given by RBM-based VMC [53]. For comparison, vanilla VQE can only achieve a relative error around the order of 10^{-3} .

Furthermore, we apply VQNHE on the molecular system H_6 -hexagon and H_6 -chain. Via symmetry enforced qubit encoding, we can simulate the corresponding system with a 10-qubit PQC and complex-RBM based post-processing module. The relative errors of optimized energy for both systems are in the order of 10^{-5} and 10^{-6} , respectively. Our VQNHE results are not only within chemical accuracy, but actually outperform CCSD method.

Discussions: The VQNHE presented in this Letter sits at the intersection between VQE and VMC [54–56]. It is similar to the VMC setup for complex-valued wavefunction, where two computational graphs are utilized:

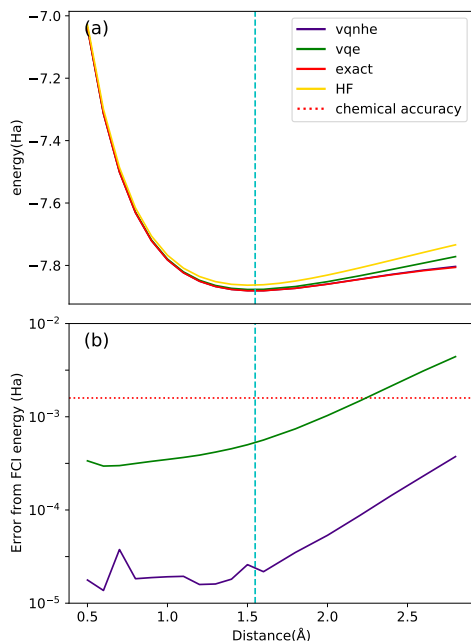


FIG. 3. LiH dissociation curve. (a) VQNHE optimized energy (purple), VQE converged energy (green), exact energy from FCI (red), Hartree-Fock energy (yellow) obtained at different bond distances with STO-3G basis set and symmetry binary encoding within complete active space. (b) Comparison of corresponding energy errors for VQNHE and VQE results. The red dash line is the threshold of chemical accuracy. VQNHE energy is always within chemical accuracy in the whole bond distance range. The cyan vertical line is the bond distance with minimum bonding energy and represents LiH molecule at equilibrium configuration.

one is for the amplitude and the other one is for the phase or sign structure. Since the quantum phase is harder to characterize than the amplitude [57–59], tensor network ansatzes have been proposed to capture such subtlety as a replacement of the neural network [60]. Within the VQNHE framework, we can view the PQC $U(\theta)$ as the part responsible to learn quantum phase, taking a similar role as the tensor networks in the VMC example described above. Since the PQC is quantum by nature, it is expected to better capture quantum entanglement and learn the quantum phase structure of the target state more efficiently. Besides, sampling from the PQC is highly efficient as it can draw independent samples each time without a high rejection ratio in traditional Metropolis-Hasting sampling strategy. Despite the similarity between VQNHE and VMC, VQNHE cannot be efficiently implemented within a VMC framework, since $\langle s|\psi\rangle$ in the denominator of E_{loc} in VMC costs exponential numbers of measurement shots to accurately estimate E_{loc} . This observation further bolsters the significance of our efficient protocol for VQNHE. In summary, the VQNHE approach can be either referred to as the neural-network enhanced VQE or as the quantum-

computing assisted VMC; it actually combines the advantages of both.

One of the promising future directions is to combine VQNHE and quantum architecture search [40, 61–66] or adaptive VQE [67–72] in which the parameterized circuit ansatz can be iteratively adjusted or grown to improve the overall performance for such a hybrid workflow. Moreover, it is worth investigating theoretically whether VQNHE is more robust against quantum noise than the vanilla VQE, as relevant evidences emerge from hardware experiments in this work.

Conclusion: In this Letter, we propose VQNHE that combines nonunitary post-processings with the PQC to improve upon VQE. VQNHE uses a hybrid representation of quantum states in order to enhance the expressive power with limited quantum hardware resources, and it consistently outperforms VQE in various tasks. We also outline a feasible protocol to implement VQNHE on real quantum hardware with rigorously proved efficiency. We demonstrate that VQE with arbitrary nonunitary post-processing can be accurately carried out with only polynomial overhead: an *exponential* improvement of efficiency that was deemed unlikely along the lines of prior proposals.

Acknowledgements: This work is supported in part by the NSFC under Grant No. 11825404 (SXZ, ZQW, and HY), the CAS Strategic Priority Research Program under Grant No. XDB28000000 (HY), and Beijing Municipal Science and Technology Commission under Grant No. Z181100004218001 (HY).

* The two authors contributed equally to this work.

† kimhsieh@tencent.com

‡ yaohong@tsinghua.edu.cn

- [1] R. P. Feynman, Simulating physics with computers, *Int. J. Theor. Phys.* **21**, 467 (1982).
- [2] M. A. Nielsen and I. L. Chuang, *Quantum Computation and Quantum Information* (Cambridge University Press, Cambridge, 2010).
- [3] J. D. Whitfield, J. Biamonte, and A. Aspuru-Guzik, Simulation of electronic structure Hamiltonians using quantum computers, *Mol. Phys.* **109**, 735 (2011).
- [4] I. M. Georgescu, S. Ashhab, and F. Nori, Quantum simulation, *Rev. Mod. Phys.* **86**, 153 (2014).
- [5] D. Wecker, B. Bauer, B. K. Clark, M. B. Hastings, and M. Troyer, Gate-count estimates for performing quantum chemistry on small quantum computers, *Phys. Rev. A - At. Mol. Opt. Phys.* **90**, 1 (2014).
- [6] J. Preskill, Quantum Computing in the NISQ era and beyond, *Quantum* **2**, 79 (2018).
- [7] S. Endo, Z. Cai, S. C. Benjamin, and X. Yuan, Hybrid quantum-classical algorithms and quantum error mitigation, *arXiv:2011.01382* (2020).
- [8] M. Cerezo, A. Arrasmith, R. Babbush, S. C. Benjamin, S. Endo, K. Fujii, J. R. McClean, K. Mitarai, X. Yuan,

- L. Cincio, and P. J. Coles, Variational Quantum Algorithms, [arXiv:2012.09265 \(2020\)](#).
- [9] K. Bharti, A. Cervera-Lierta, T. H. Kyaw, T. Haug, S. Alperin-Lea, A. Anand, M. Degroote, H. Heimonen, J. S. Kottmann, T. Menke, W.-K. Mok, S. Sim, L.-C. Kwek, and A. Aspuru-Guzik, Noisy intermediate-scale quantum (NISQ) algorithms, [arXiv:2101.08448 \(2021\)](#).
- [10] A. Peruzzo, J. McClean, P. Shadbolt, M.-H. Yung, X.-Q. Zhou, P. J. Love, A. Aspuru-Guzik, and J. L. O'Brien, A variational eigenvalue solver on a photonic quantum processor, *Nat. Commun.* **5**, 4213 (2014).
- [11] P. J. J. O'Malley, R. Babbush, I. D. Kivlichan, J. Romero, J. R. McClean, R. Barends, J. Kelly, P. Roushan, A. Tranter, N. Ding, B. Campbell, Y. Chen, Z. Chen, B. Chiaro, A. Dunsworth, A. G. Fowler, E. Jeffrey, E. Lucero, A. Megrant, J. Y. Mutus, M. Neeley, C. Neill, C. Quintana, D. Sank, A. Vainsencher, J. Wenner, T. C. White, P. V. Coveney, P. J. Love, H. Neven, A. Aspuru-Guzik, and J. M. Martinis, Scalable Quantum Simulation of Molecular Energies, *Phys. Rev. X* **6**, 031007 (2016).
- [12] J. R. McClean, J. Romero, R. Babbush, and A. Aspuru-Guzik, The theory of variational hybrid quantum-classical algorithms, *New J. Phys.* **18**, 023023 (2016).
- [13] C. Hempel, C. Maier, J. Romero, J. McClean, T. Monz, H. Shen, P. Jurcevic, B. P. Lanyon, P. Love, R. Babbush, A. Aspuru-Guzik, R. Blatt, and C. F. Roos, Quantum Chemistry Calculations on a Trapped-Ion Quantum Simulator, *Phys. Rev. X* **8**, 31022 (2018).
- [14] J.-G. Liu, Y.-H. Zhang, Y. Wan, and L. Wang, Variational quantum eigensolver with fewer qubits, *Phys. Rev. Res.* **1**, 023025 (2019).
- [15] Y. Cao, J. Romero, J. P. Olson, M. Degroote, P. D. Johnson, M. Kieferová, I. D. Kivlichan, T. Menke, B. Peropadre, N. P. D. Sawaya, S. Sim, L. Veis, and A. Aspuru-Guzik, Quantum Chemistry in the Age of Quantum Computing, *Chem. Rev.* **119**, 10856 (2019).
- [16] S. McArdle, S. Endo, A. Aspuru-Guzik, S. C. Benjamin, and X. Yuan, Quantum computational chemistry, *Rev. Mod. Phys.* **92**, 015003 (2020).
- [17] B. Bauer, S. Bravyi, M. Motta, and G. Kin-Lic Chan, Quantum Algorithms for Quantum Chemistry and Quantum Materials Science, *Chem. Rev.* **120**, 12685 (2020).
- [18] O. Higgott, D. Wang, and S. Brierley, Variational Quantum Computation of Excited States, *Quantum* **3**, 156 (2019).
- [19] K. M. Nakanishi, K. Mitarai, and K. Fujii, Subspace-search variational quantum eigensolver for excited states, *Phys. Rev. Res.* **1**, 033062 (2019).
- [20] Y. Li and S. C. Benjamin, Efficient Variational Quantum Simulator Incorporating Active Error Minimization, *Phys. Rev. X* **7**, 021050 (2017).
- [21] X. Yuan, S. Endo, Q. Zhao, Y. Li, and S. C. Benjamin, Theory of variational quantum simulation, *Quantum* **3**, 191 (2019).
- [22] S. McArdle, T. Jones, S. Endo, Y. Li, S. C. Benjamin, and X. Yuan, Variational ansatz-based quantum simulation of imaginary time evolution, *npj Quantum Inf.* **5**, 75 (2019).
- [23] C. Cirstoiu, Z. Holmes, J. Iosue, L. Cincio, P. J. Coles, and A. Sornborger, Variational fast forwarding for quantum simulation beyond the coherence time, *npj Quantum Inf.* **6**, 82 (2020).
- [24] S.-H. Lin, R. Dilip, A. G. Green, A. Smith, and F. Pollmann, Real- and imaginary-time evolution with compressed quantum circuits, [arXiv:2008.10322 \(2020\)](#).
- [25] S. Endo, J. Sun, Y. Li, S. C. Benjamin, and X. Yuan, Variational Quantum Simulation of General Processes, *Phys. Rev. Lett.* **125**, 010501 (2020).
- [26] M. Benedetti, M. Fiorentini, and M. Lubasch, Hardware-efficient variational quantum algorithms for time evolution, [arXiv:2009.12361 \(2020\)](#).
- [27] C.-K. Lee, P. Patil, S. Zhang, and C.-Y. Hsieh, A Neural-Network Variational Quantum Algorithm for Many-Body Dynamics, [arXiv:2008.13329 \(2020\)](#).
- [28] F. Arute, K. Arya, R. Babbush, D. Bacon, J. C. Bardin, R. Barends, R. Biswas, S. Boixo, F. G. S. L. Brandao, D. A. Buell, B. Burkett, Y. Chen, Z. Chen, B. Chiaro, R. Collins, W. Courtney, A. Dunsworth, E. Farhi, B. Foxen, A. Fowler, C. Gidney, M. Giustina, R. Graff, K. Guerin, S. Habegger, M. P. Harrigan, M. J. Hartmann, A. Ho, M. Hoffmann, T. Huang, T. S. Humble, S. V. Isakov, E. Jeffrey, Z. Jiang, D. Kafri, K. Kechedzhi, J. Kelly, P. V. Klimov, S. Knysh, A. Korotkov, F. Kostritsa, D. Landhuis, M. Lindmark, E. Lucero, D. Lyakh, S. Mandrà, J. R. McClean, M. McEwen, A. Megrant, X. Mi, K. Michielsen, M. Mohseni, J. Mutus, O. Naaman, M. Neeley, C. Neill, M. Y. Niu, E. Ostby, A. Petukhov, J. C. Platt, C. Quintana, E. G. Rieffel, P. Roushan, N. C. Rubin, D. Sank, K. J. Satzinger, V. Smelyanskiy, K. J. Sung, M. D. Trevithick, A. Vainsencher, B. Villalonga, T. White, Z. J. Yao, P. Yeh, A. Zalcman, H. Neven, and J. M. Martinis, Quantum supremacy using a programmable superconducting processor, *Nature* **574**, 505 (2019).
- [29] H.-S. Zhong, H. Wang, Y.-H. Deng, M.-C. Chen, L.-C. Peng, Y.-h. Luo, J. Qin, D. Wu, X. Ding, Y. Hu, P. Hu, X.-y. Yang, W.-j. Zhang, H. Li, Y. Li, X. Jiang, L. Gan, G. Yang, L. You, Z. Wang, L. Li, N.-l. Liu, C.-y. Lu, and J.-w. Pan, Quantum computational advantage using photons, *Science* **370**, 1460 (2020).
- [30] A. G. Taube and R. J. Bartlett, New perspectives on unitary coupled-cluster theory, *Int. J. Quantum Chem.* **106**, 3393 (2006).
- [31] D. Wecker, M. B. Hastings, and M. Troyer, Progress towards practical quantum variational algorithms, *Phys. Rev. A* **92**, 042303 (2015).
- [32] A. Kandala, A. Mezzacapo, K. Temme, M. Takita, M. Brink, J. M. Chow, and J. M. Gambetta, Hardware-efficient variational quantum eigensolver for small molecules and quantum magnets, *Nature* **549**, 242 (2017).
- [33] A. J. McCaskey, Z. P. Parks, J. Jakowski, S. V. Moore, T. D. Morris, T. S. Humble, and R. C. Pooser, Quantum chemistry as a benchmark for near-term quantum computers, *npj Quantum Inf.* **5**, 99 (2019).
- [34] J.-G. Liu and L. Wang, Differentiable learning of quantum circuit Born machines, *Phys. Rev. A* **98**, 062324 (2018).
- [35] J.-G. Liu, L. Mao, P. Zhang, and L. Wang, Solving quantum statistical mechanics with variational autoregressive networks and quantum circuits, *Mach. Learn. Sci. Technol.* **2**, 025011 (2021).
- [36] G. Verdon, J. Marks, S. Nanda, S. Leichenauer, and J. Hidary, Quantum Hamiltonian-Based Models and the Variational Quantum Thermalizer Algorithm, [arXiv:1910.02071 \(2019\)](#).
- [37] C. Y. Hsieh, Q. Sun, S. Zhang, and C. K. Lee, Unitary-

- coupled restricted Boltzmann machine ansatz for quantum simulations, *npj Quantum Inf.* **7**, 19 (2021).
- [38] M. Benedetti, B. Coyle, M. Fiorentini, M. Lubasch, and M. Rosenkranz, Variational inference with a quantum computer, [arXiv:2103.06720](https://arxiv.org/abs/2103.06720) (2021).
- [39] G. Li, Z. Song, and X. Wang, VSQ: Variational Shadow Quantum Learning for Classification, [arXiv:2012.08288](https://arxiv.org/abs/2012.08288) (2020).
- [40] S.-X. Zhang, C.-Y. Hsieh, S. Zhang, and H. Yao, Neural Predictor based Quantum Architecture Search, [arXiv:2103.06524](https://arxiv.org/abs/2103.06524) (2021).
- [41] G. Mazzola, P. J. Ollitrault, P. K. Barkoutsos, and I. Tavernelli, Nonunitary Operations for Ground-State Calculations in Near-Term Quantum Computers, *Phys. Rev. Lett.* **123**, 130501 (2019).
- [42] R. Jastrow, Many-body problem with strong forces, *Phys. Rev.* **98**, 1479 (1955).
- [43] A. Zen, E. Coccia, Y. Luo, S. Sorella, and L. Guidoni, Static and dynamical correlation in diradical molecules by quantum monte carlo using the jastrow antisymmetrized geminal power ansatz, *J. Chem. Theory Comput.* **10**, 1048 (2014).
- [44] C. Genovese, A. Meninno, and S. Sorella, Assessing the accuracy of the Jastrow antisymmetrized geminal power in the H 4 model system, *J. Chem. Phys.* **150**, 084102 (2019).
- [45] F. Benfenati, G. Mazzola, C. Capecchi, P. K. Barkoutsos, P. J. Ollitrault, I. Tavernelli, and L. Guidoni, Improved accuracy on noisy devices by non-unitary Variational Quantum Eigensolver for chemistry applications, [arXiv:2101.09316](https://arxiv.org/abs/2101.09316) (2021).
- [46] J. Li, X. Yang, X. Peng, and C.-P. Sun, Hybrid Quantum-Classical Approach to Quantum Optimal Control, *Phys. Rev. Lett.* **118**, 150503 (2017).
- [47] K. Mitarai, M. Negoro, M. Kitagawa, and K. Fujii, Quantum circuit learning, *Phys. Rev. A* **98**, 032309 (2018).
- [48] M. Schuld, V. Bergholm, C. Gogolin, J. Izaac, and N. Killoran, Evaluating analytic gradients on quantum hardware, *Phys. Rev. A* **99**, 032331 (2019).
- [49] The open source implementation of VQNHE can be found at <https://github.com/refraction-ray/tensorcircuit>.
- [50] J. M. Turney, A. C. Simmonett, R. M. Parrish, E. G. Hohenstein, F. A. Evangelista, J. T. Fermann, B. J. Mintz, L. A. Burns, J. J. Wilke, M. L. Abrams, N. J. Russ, M. L. Leininger, C. L. Janssen, E. T. Seidl, W. D. Allen, H. F. Schaefer, R. A. King, E. F. Valeev, C. D. Sherrill, and T. D. Crawford, Psi4: An open-source ab initio electronic structure program, *Wiley Interdiscip. Rev. Comput. Mol. Sci.* **2**, 556 (2012).
- [51] J. R. McClean, K. J. Sung, I. D. Kivlichan, Y. Cao, C. Dai, E. S. Fried, C. Gidney, B. Gimby, P. Gokhale, T. Häner, T. Hardikar, V. Havlíček, O. Higgott, C. Huang, J. Izaac, Z. Jiang, X. Liu, S. McArdle, M. Neeley, T. O’Brien, B. O’Gorman, I. Ozfidan, M. D. Radin, J. Romero, N. Rubin, N. P. D. Sawaya, K. Setia, S. Sim, D. S. Steiger, M. Staudtner, Q. Sun, W. Sun, D. Wang, F. Zhang, and R. Babbush, OpenFermion: The Electronic Structure Package for Quantum Computers, [arXiv:2017.08057](https://arxiv.org/abs/2017.08057) (2017).
- [52] M. Staudtner and S. Wehner, Fermion-to-qubit mappings with varying resource requirements for quantum simulation, *New J. Phys.* **20**, 063010 (2018).
- [53] K. Choo, A. Mezzacapo, and G. Carleo, Fermionic neural-network states for ab-initio electronic structure, *Nat. Commun.* **11**, 2368 (2020).
- [54] W. L. McMillan, Ground State of Liquid He4, *Phys. Rev.* **138**, A442 (1965).
- [55] D. Ceperley, G. V. Chester, and M. H. Kalos, Monte Carlo simulation of a many-fermion study, *Phys. Rev. B* **16**, 3081 (1977).
- [56] G. Carleo and M. Troyer, Solving the quantum many-body problem with artificial neural networks, *Science* **355**, 602 (2017).
- [57] T. Westerhout, N. Astrakhantsev, K. S. Tikhonov, M. I. Katsnelson, and A. A. Bagrov, Generalization properties of neural network approximations to frustrated magnet ground states, *Nat. Commun.* **11**, 1593 (2020).
- [58] M. Bukov, M. Schmitt, and M. Dupont, Learning the ground state of a non-stoquastic quantum Hamiltonian in a rugged neural network landscape, [arXiv:2011.11214](https://arxiv.org/abs/2011.11214) (2020).
- [59] C.-Y. Park and M. J. Kastoryano, Are neural quantum states good at solving non-stoquastic spin Hamiltonians?, [arXiv:2012.08889](https://arxiv.org/abs/2012.08889) (2020).
- [60] X. Liang, S.-J. Dong, and L. He, Hybrid convolutional neural network and projected entangled pair states wave functions for quantum many-particle states, *Phys. Rev. B* **103**, 035138 (2021).
- [61] S.-X. Zhang, C.-Y. Hsieh, S. Zhang, and H. Yao, Differentiable Quantum Architecture Search, [arXiv:2010.08561](https://arxiv.org/abs/2010.08561) (2020).
- [62] L. Li, M. Fan, M. Coram, P. Riley, and S. Leichenauer, Quantum optimization with a novel Gibbs objective function and ansatz architecture search, *Phys. Rev. Res.* **2**, 023074 (2020).
- [63] Y. Du, T. Huang, S. You, M.-H. Hsieh, and D. Tao, Quantum circuit architecture search: error mitigation and trainability enhancement for variational quantum solvers, [arXiv:2010.10217](https://arxiv.org/abs/2010.10217) (2020).
- [64] Z. Lu, P.-X. Shen, and D.-L. Deng, Markovian Quantum Neuroevolution for Machine Learning, [arXiv:2012.15131](https://arxiv.org/abs/2012.15131) (2020).
- [65] M. Bilkis, M. Cerezo, G. Verdon, P. J. Coles, and L. Cincio, A semi-agnostic ansatz with variable structure for quantum machine learning, [arXiv:2103.06712](https://arxiv.org/abs/2103.06712) (2021).
- [66] E.-J. Kuo, Y.-L. L. Fang, and S. Y.-C. Chen, Quantum Architecture Search via Deep Reinforcement Learning, [arXiv:2104.07715](https://arxiv.org/abs/2104.07715) (2021).
- [67] H. R. Grimsley, S. E. Economou, E. Barnes, and N. J. Mayhall, An adaptive variational algorithm for exact molecular simulations on a quantum computer, *Nat. Commun.* **10**, 3007 (2019).
- [68] A. G. Rattew, S. Hu, M. Pistoia, R. Chen, and S. Wood, A Domain-agnostic, Noise-resistant, Hardware-efficient Evolutionary Variational Quantum Eigensolver, [arXiv:1910.09694](https://arxiv.org/abs/1910.09694) (2019).
- [69] D. Chivilikhin, A. Samarin, V. Ulyantsev, I. Iorsh, A. R. Oganov, and O. Kyriienko, MoG-VQE: Multiobjective genetic variational quantum eigensolver, [arXiv:2007.04424](https://arxiv.org/abs/2007.04424) (2020).
- [70] Y. S. Yordanov, V. Armaos, C. H. Barnes, and D. R. Arvidsson-Shukur, Iterative qubit-excitation based variational quantum eigensolver, [arXiv:2011.10540](https://arxiv.org/abs/2011.10540) (2020).
- [71] S. Sim, J. Romero, J. F. Gonthier, and A. A. Kunitsa, Adaptive pruning-based optimization of parameterized quantum circuits, [arXiv:2010.00629](https://arxiv.org/abs/2010.00629) (2020).

SUPPLEMENTAL MATERIALS
Measurement efficiency for VQNHE

As shown in the main text, the overhead of quantum hardware resources for VQNHE is at most $m-1$ two-qubit gates where $m \leq n$ is the number of X and Y operators present in the Pauli string \hat{H} . Furthermore, our proposed protocol is also unbiased without any systematic deviations from the ground truth. Therefore, the only concern left is: how many measurement shots are required to estimate the energy expectation at a given precision? If the number of shots required is only polynomial times more than the original VQE measurements, then we may conclude that VQNHE is efficient and exponentially faster than previous proposals attempting to incorporate nonunitary post-processing with VQE.

For the vanilla VQE, assuming that there is probability p to measure \hat{H} with +1 result, then the standard deviation for the estimation after N measurement shots is:

$$\delta\langle\hat{H}\rangle = \frac{2\sqrt{p(1-p)}}{\sqrt{N}}, \quad (\text{S1})$$

which is due to the deviation formula for the binomial distribution. Therefore, to achieve an accuracy of $1 - \varepsilon$, we have to measure the system at least $N = \frac{4p(1-p)}{\varepsilon^2}$ times. The hardest case is when $\langle\hat{H}\rangle = 0$ with $p = 1/2$, and the required number of measurement shots is in the order of $\frac{1}{\varepsilon^2}$.

Next, we turn to VQNHE, the expectation value is computed as a fraction of two quantities, $\langle\hat{H}\rangle = n/d$, where $d = E_{p(s)}(f^2(s))$ and $n = E_{q(s)}((1-2s_0)f(0s_{1:n-1})f(1s_{1:n-1}))$. $p(s)$ and $q(s)$ are two distributions determined by the output state of two different PQCs U and VU . Considering the standard deviation, we have:

$$\delta\langle\hat{H}\rangle = \delta\left(\frac{n}{d}\right) < \left|\frac{\delta n}{d\sqrt{N}}\right| + \left|\frac{\delta d n}{d^2\sqrt{N}}\right|, \quad (\text{S2})$$

where δn and δd are the standard deviation of the random variable in the denominator and numerator. Recall $\langle\hat{H}\rangle = n/d < 1$ and suppose the neural function f is restricted in the range $[1/r, r]$, then we have $\frac{1}{d} \leq r^2$, $\delta d < (r^2 - 1/r^2)/2$, $\delta n < 2r^2\sqrt{p(1-p)}$ and

$$\delta\langle\hat{H}\rangle < \frac{1}{\sqrt{N}}\left(\frac{\delta d + \delta n}{d}\right) < \frac{3r^4}{2\sqrt{N}}. \quad (\text{S3})$$

Therefore, the required number of shots to attain the same accuracy ε is at most $N = \frac{9}{4}r^8/\varepsilon^2$.

We can further tight the bound by more thorough analysis. In terms of the first term:

$$\left(\frac{\delta d}{d}\right)^2 = \frac{\langle f^4(s) \rangle_s}{\langle f^2(s) \rangle_s^2} - 1, \quad (\text{S4})$$

where the expectation is defined by bitstring s collected from the PQC U . The upper bound of Eq. (S4) is reached when $f(s)$ is a two-value function always giving r or $1/r$. This is because, otherwise, pairs of $f(s_1)$ and $f(s_2)$ of values in $(1/r, r)$ can be pushed to two sides in a way that leaves $E(f^2(s))$ unchanged until one of the two f values is now in the boundary. This ‘‘push’’ procedure keeps the denominator of Eq. (S4) unchanged while monotonically increases the numerator of Eq. (S4). Therefore, we have:

$$\left(\frac{\delta d}{d}\right)^2 \leq \max_p \frac{pr^4 + (1-p)1/r^4}{(pr^2 + (1-p)/r^2)^2} - 1 = \frac{r^4}{4} + \frac{1}{4r^4} + \frac{1}{2} - 1, \quad (\text{S5})$$

where p is the total probability to measure $\{s|f(s) = r\}$. Hence,

$$\frac{\delta d}{d} \leq \frac{1}{2}\left(r^2 - \frac{1}{r^2}\right). \quad (\text{S6})$$

We now focus on the second term $\delta n/d$. We define the probability $p_{s_{1:n-1}} = |\langle 0s_{1:n-1}|\psi\rangle|^2 + |\langle 1\widetilde{s}_{1:n-1}|\psi\rangle|^2$, where $|\psi\rangle$ is the wavefunction from the PQC U . In the numerator, we require the probability amplitude of $\psi_{\pm, s_{1:n-1}} = \langle \pm, s_{1:n-1}|\psi\rangle$ which is just $\frac{1}{\sqrt{2}}(\langle 0s_{1:n-1}|\psi\rangle \pm S(1\widetilde{s}_{1:n-1})\langle 1\widetilde{s}_{1:n-1}|\psi\rangle)$. We define the normalized probability amplitude as:

$$\phi_{\pm, s_{1:n-1}} = \frac{1}{\sqrt{p_{s_{1:n-1}}}}\psi_{\pm, s_{1:n-1}} = \frac{1}{\sqrt{2p_{s_{1:n-1}}}}(\langle 0s_{1:n-1}|\psi\rangle \pm S(1\widetilde{s}_{1:n-1})\langle 1\widetilde{s}_{1:n-1}|\psi\rangle), \quad (\text{S7})$$

with $p_{s_{1:n-1}}^{-1/2}$ as the normalization factor. We then have $|\phi_{+, s_{1:n-1}}|^2 + |\phi_{-, s_{1:n-1}}|^2 = 1$. Namely, to accommodate the probability distribution in the numerator and the denominator, we recast the distribution freedom as a classical part $p_{s_{1:n-1}}$ and a quantum part $\phi_{\pm, s_{1:n-1}}$. These two parts are decoupled and vary independently. We now have:

$$\left(\frac{\delta n}{d}\right)^2 = \frac{\langle ((1-2s_0)f(0s_{1:n-1})f(1\widetilde{s}_{1:n-1}))^2 \rangle_{UV}}{\langle f^2(s) \rangle_U^2} - \langle \hat{H} \rangle^2 \leq \frac{\langle (f(0s_{1:n-1})f(1\widetilde{s}_{1:n-1}))^2 \rangle_{UV}}{\langle f^2(s) \rangle_U^2}, \quad (\text{S8})$$

where we have utilized the fact that $\langle \hat{H} \rangle^2 \in [0, 1]$. The expectation denoted by $\langle \cdot \rangle_{UV}$ and $\langle \cdot \rangle_U$ is computed by the measured bitstrings from the PQC U with and without the measurement circuit V . Note the probability to get s from the PQC U is $\frac{p_{s_{1:n-1}}}{2}|\phi_{+, s_{1:n-1}}|^2 + (1-2s_0)|\phi_{-, s_{1:n-1}}|^2$:

$$\begin{aligned} \left(\frac{\delta n}{d}\right)^2 &\leq \frac{\sum_{0s_{1:n-1}} p_{s_{1:n-1}} f^2(0s_{1:n-1}) f^2(1\widetilde{s}_{1:n-1})}{1/4(\sum_{0s_{1:n-1}} p_{s_{1:n-1}} (f^2(0s_{1:n-1})|\phi_+ + \phi_-|^2 + f^2(1\widetilde{s}_{1:n-1})|\phi_+ - \phi_-|^2)^2} \\ &= 4 \frac{\sum_{0s_{1:n-1}} p_{s_{1:n-1}} f^2(0s_{1:n-1}) f^2(1\widetilde{s}_{1:n-1})}{(\sum_{0s_{1:n-1}} p_{s_{1:n-1}} (f^2(0s_{1:n-1}) + f^2(1\widetilde{s}_{1:n-1}) + 2(f^2(0s_{1:n-1}) - f^2(1\widetilde{s}_{1:n-1})) \text{Re}(\phi_+^* \phi_-))^2}. \end{aligned} \quad (\text{S9})$$

Since ϕ_{\pm} is only in the denominator, we let $2\text{Re}(\phi_+^* \phi_-) = -\text{sign}(f^2(0s) - f^2(1\tilde{s}))$ to make the denominator as small as possible (we use $0s$ and $1\tilde{s}$ as the shortcut for $0s_{1:n-1}$ and $1\widetilde{s}_{1:n-1}$, respectively). We now have:

$$\begin{aligned} \left(\frac{\delta n}{d}\right)^2 &\leq \frac{\sum_{0s} p_s f^2(0s) f^2(1\tilde{s})}{(\sum_{0s} p_s \min(f(0s), f(1\tilde{s}))^2)^2} \\ &= \frac{\sum_{0s} p_s f^2(0s) f^2(1\tilde{s})}{\sum_{0s} p_s \min(f(0s), f(1\tilde{s}))^2} \frac{1}{\sum_{0s} p_s \min(f(0s), f(1\tilde{s}))^2} \\ &\leq r^2 \frac{\sum_{0s} p_s f^2(0s) f^2(1\tilde{s})}{\sum_{0s} p_s \min(f(0s), f(1\tilde{s}))^2}. \end{aligned} \quad (\text{S10})$$

Without loss of generality, we assume $f(1\tilde{s}) > f(0s)$ for each $s_{1:n-1}$, then we let $f(1\tilde{s}) = r$ to maximize the above formula:

$$\left(\frac{\delta n}{d}\right)^2 \leq r^4 \frac{\sum_{0s} p_s f^2(0s)}{\sum_{0s} p_s f^2(0s)} = r^4. \quad (\text{S11})$$

To sum up, we have:

$$\delta \langle \hat{H} \rangle < \frac{1}{\sqrt{N}} \left(\frac{\delta d + \delta n}{d} \right) \leq \frac{1}{\sqrt{N}} \left(\frac{r^2}{2} - \frac{1}{2r^2} + r^2 \right) \leq \frac{1}{\sqrt{N}} \frac{3r^2}{2}. \quad (\text{S12})$$

Therefore, the required number of measurement shots to reach the accuracy $1 - \varepsilon$ is at most $N = \frac{9r^4}{4\varepsilon^2}$.

This bound is tight in terms of the scaling with r , as one can devise f and the PQC U such that the bound saturates. The extra overhead for VQNHE (with respect to VQE) is only polynomial in terms of the cutoff r and independent of the system size N . Therefore, VQNHE is highly efficient compared to previous proposals that require an exponential amount of resources. In actual experiments, as long as the output of f is restricted to a reasonable range, the overhead should be much smaller than the one indicated by the upper bound here. This is because, in real problems, the distribution p based on the wavefunction and the distribution of f value over the bitstring space is not that extreme.

VQNHE formalism with complex neural function

In this section, we show an efficient measurement protocol for complex-valued neural post-processing as a complement to the result in the main text. We have:

$$\begin{aligned}
& \langle \psi_f | \hat{H} | \psi_f \rangle \\
&= \langle \psi | \left(\sum_{s \in 0s_{1:n-1}} f^*(s) f(\tilde{s}) S(s) |s\rangle \langle \tilde{s}| + f(s) f^*(\tilde{s}) S(\tilde{s}) |\tilde{s}\rangle \langle s| \right) | \psi \rangle \\
&= \langle \psi | \sum_{s \in 0s_{1:n-1}} R(s) (S(s) |s\rangle \langle \tilde{s}| + S(\tilde{s}) |\tilde{s}\rangle \langle s|) + iI(s) (S(s) |s\rangle \langle \tilde{s}| - S(\tilde{s}) |\tilde{s}\rangle \langle s|) | \psi \rangle, \tag{S13}
\end{aligned}$$

where $R(s) = \text{Re}(f^*(s)f(\tilde{s}))$ and $I(s) = \text{Im}(f^*(s)f(\tilde{s}))$. For the first term in the last line of Eq. (S13), one may simply use the measurement and estimation protocol given in the main text with a simple replacement: substituting $f(0s_{1:n-1})f(\widetilde{1s_{1:n-1}})$ with $\text{Re}(f(0s_{1:n-1})f(\widetilde{1s_{1:n-1}}))$.

We now focus on the second term in the last line of Eq. (S13),

$$\begin{aligned}
& \langle \psi | \sum_{s \in 0s_{1:n-1}} iI(s) (S(s) |s\rangle \langle \tilde{s}| - S(\tilde{s}) |\tilde{s}\rangle \langle s|) | \psi \rangle \\
&= \langle \psi | \sum_{s \in 0s_{1:n-1}} I(s) [|+, s'\rangle \langle +, s'| - |-, s'\rangle \langle -, s'|] | \psi \rangle \\
&= \sum_{s \in 0s_{1:n-1}} (|\psi'_{+,s}\rangle^2 I(s) + |\psi'_{-,s}\rangle^2 (-I(s))), \tag{S14}
\end{aligned}$$

where $\psi'_{\pm,s} = \langle \pm, s' | \psi \rangle$ are the amplitudes associated with a new basis $|\pm, s_{1:n-1}\rangle'$:

$$\begin{aligned}
|+, s_{1:n-1}\rangle' &= \frac{1}{\sqrt{2}} (-iS(s) |0s_{1:n-1}\rangle - |\widetilde{1s_{1:n-1}}\rangle) \\
|-, s_{1:n-1}\rangle' &= \frac{1}{\sqrt{2}} (-iS(s) |0s_{1:n-1}\rangle + |\widetilde{1s_{1:n-1}}\rangle). \tag{S15}
\end{aligned}$$

Therefore, to measure the contribution from the imaginary part of f , we need another measurement circuit V' such that $(V')^\dagger |s\rangle \propto |\pm, s_{1:n-1}\rangle' \propto \frac{1}{\sqrt{2}} (-i |0s_{1:n-1}\rangle - (1 - 2s_0) \hat{H} |0s_{1:n-1}\rangle)$. Clearly, V' can be constructed with minor modifications of our proposed method to build V in the main text. Firstly, we still have to locate the star qubit and apply control-X/Y/Z gates on all other qubits involved in the Pauli string \hat{H} . The only difference is that we measure in the X(-Y) basis for the star qubit when the operator is Y(X) in the \hat{H} . In other words, we apply Hadamard gate on the star qubit if Y operator is present in \hat{H} , and apply $\text{Rx} = \exp(\pi/4 iX)$ on the star qubit if X operator is present. In short, the protocol to estimate the expectation value from quantum-neural hybrid state costs only twice the processing time as the case for the real-valued f .

Technical details for the simulation of quantum spin systems

1D TFIM and Heisenberg model with 12 sites and periodic boundary conditions are evaluated by both VQE and VQNHE. The quantum ansatz used in the TFIM case is a multiple parameter version of the QAOA ansatz with alternating ZZ and X layers:

$$U(\boldsymbol{\theta}) = \prod_{p=1}^2 \left(\prod_{i=1}^{12} e^{i\theta_{ip,x} X_i} \prod_{i=1}^{12} e^{i\theta_{ip,zz} Z_i Z_{(i+1)\%12}} \right) \prod_{i=1}^{12} H_i, \tag{S16}$$

where H_i is the Hadamard gate on the i -th qubit.

The PQC we utilized in the main text for isotropic Heisenberg model is built with layers of parametrized swap gates with pairs of Bell states as the input. Specifically, we have:

$$U(\boldsymbol{\theta}) |0^{12}\rangle = \prod_{p=1}^2 \left(\prod_{i=1}^{12} e^{i\theta_{ip} \text{SWAP}_{i,i+1}} \right) \prod_{i=1}^6 \left(\frac{|01\rangle - |10\rangle}{\sqrt{2}} \right), \tag{S17}$$

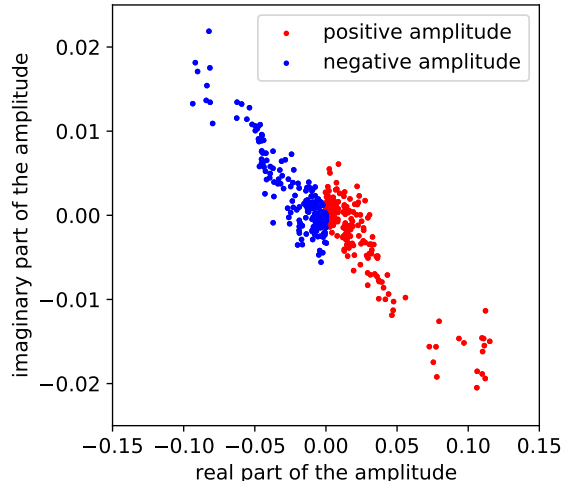


FIG. S1. Sign structure learned by the PQC in VQNHE setup. The scatter points represent the amplitude components on the computational basis from the optimized PQC wavefunction: real and imaginary parts are shown. The color on each point stands for the sign of the exact ground state. As we can see, the PQC roughly learns about the sign structure of Heisenberg model’s ground state up to a phase.

where $\text{SWAP} = \frac{1}{2}(X_1X_2 + Y_1Y_2 + Z_1Z_2 + I_1I_2)$. This ansatz conserves the $\text{SU}(2)$ symmetry for the isotropic Heisenberg model and thus keep the variational state in the same symmetry sector as the ground state.

The classical neural model we utilized is a real-valued fully connected neural network with two hidden layers of width 24 and 12 with ReLU activation (we attach one more 24-unit hidden layer for the Heisenberg model). The final scalar output is activated via $e^{\phi_0 \tanh(*)}$, where ϕ_0 is a trainable weight that regulates the output range of f and, in turn, controls the magnitude of fluctuations for VQNHE estimation. By restricting the range or the maximum value of f , we can keep the measurement overhead for VQNHE estimation as low as possible while witnessing just a slightly worse performance. This is a classic trade-off. Nonetheless, we report the result for a Heisenberg model with $\phi_0 < 1$ imposed and $f \in [1/e, e]$ is guaranteed. The required number of measurement shots for the given accuracy is only three times more than that for the original VQE. And the approximation ratio in the result is still very good: VQNHE gives -21.53 (0.1% in relative error) for the ground-state energy of the Heisenberg model, which is still much better than the vanilla VQE results (given by an ansatz with 2-layer parameterized swap gates).

For the same Heisenberg model, we also report VQE and VQNHE results given by the hardware efficient ansatz ($[\text{Rx}, \text{Rz}, \text{CNOT}]^*2$). The naïve VQE gives the converged energy -19.26 while VQNHE gives the converged energy -21.30 . The performance boost compared to VQE is more significant when we do not explicitly impose symmetry in the circuit architecture.

It is also interesting to observe how the PQC incorporates the phase structure of Heisenberg model’s ground state function. Since without transformation of YY coupling, the ground state of Heisenberg model shows a sign structure. The relevant information learned by the PQC in a VQNHE setup is shown in Fig. S1.

In addition, we comment on the joint training of quantum and classical modules. Firstly, the parameters in the PQC and the neural network should be updated with different optimizers as the learning tend to progress at different scales. We choose Adam optimizer for all simulations in this work. Secondly, we observe that the naïve joint training and stage-wise training where the PQC and the neural network get optimized sequentially, are both inferior optimization approaches. Instead, a much better solution is to optimize the PQC first then follows by a joint optimization on both the PQC and the neural network (but the PQC receives a much smaller learning rate in the second stage). An example of the learning curves for both optimizers (PQC and neural network) is displayed in Fig. S4.

Technical details for quantum hardware experiments

We use the 1D 5-site TFIM model with open boundary condition as the test system, since the quantum hardware provided by IBM (specifically we use IBM_Santiago instance) shows a one dimensional connectivity. The exact ground

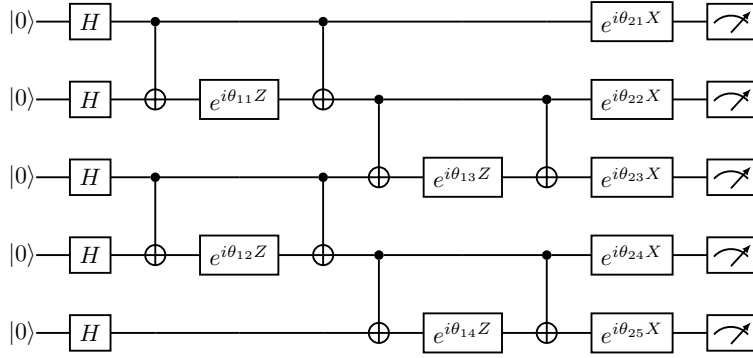


FIG. S2. The PQC ansatz utilized in the task to simulate the 5-site TFIM model for both VQE and VQNHE. This quantum circuit is evaluated on noiseless simulator, noisy simulator and quantum hardware IBM_Santiago.

state energy for this model obtained from exact diagonalization is -6.02667418 . The PQC we utilized in both VQE and VQNHE experiments are shown in Fig. S2. In the design of the PQC, the number of two-qubit gates is kept small for high-fidelity results, as the quantum error brought by two-qubit gates is rather large in real hardware. So we only keep one layer of $e^{i\theta Z_i Z_j}$ gates. The classical neural model in the VQNHE setup is a real-valued fully connected neural network with two hidden layers of 10 and 20 units, and the activations for the two layers are ReLU and sigmoid, respectively. The final scalar output is further activated via $e^{\phi_0 \tanh(*)}$.

Since the quantum-classical hybrid optimization process is rather time consuming to run in real quantum hardware, we first optimize both VQE and VQNHE using the ideal simulator without measurement uncertainty and quantum noise to obtain the corresponding optimal parameters for the PQC and the classical model. The ideal converged energies for both VQE and VQNHE are -5.897229 (relative error $2 * 10^{-2}$) and -6.02667418 (relative error $2 * 10^{-12}$), respectively. If we run the corresponding PQC on noiseless simulator, the results obtained from bitstrings have standard deviations originated from measurement uncertainty while the mean values stay the same as the ideal cases within the error bar for both cases. The number for measurement shots in each group is 8192: namely, we run 100 groups of independent measurements and report the mean and standard deviation among these groups of measurement results. The mean value and standard deviation pairs for both VQE and VQNHE in noiseless simulator are: $(-5.895, 0.0207)$, $(-6.023, 0.0236)$. Note that the bitstrings measured in the VQE case are ZZZZZ and XXXXX while the bitstrings measured in the VQNHE case are ZZZZZ, XZZZZ, ZXZZZ, ZZZZZ, ZZZXZ, ZZZZX.

Things become more interesting when quantum noise sets in, such as noisy simulators and the real quantum hardware. Note that the noisy simulator we utilized in Qiskit is also characterized by the noise model for IBM_Santiago. In terms of the standard VQE, the simulation and data processing from measured bitstrings are similar as the noiseless case. The only add-on is that we apply measurement error mitigation for all results from noisy simulator and real quantum hardware. This QEM technique is provided by Qiskit: <https://qiskit.org/textbook/ch-quantum-hardware/measurement-error-mitigation.html>. We compare the results from 100 groups of measurements in the simulator case and 10 groups of measurements in the real hardware. Each group contains 8192 measurement shots. The mean and standard deviation pairs from the quantum simulator and hardware cases are $(-5.724, 0.0282)$ and $(-5.690, 0.0228)$, respectively. On the other hand, when we run the VQNHE in noisy settings, the result obtained from the ideal optimal post-processing on the obtained measurements is not optimal anymore. This is because the neural network is trained in ideal scenario and doesn't incorporate the appropriate noise model in quantum hardware. Therefore, retraining on the neural network is required based on the results from measurement bitstrings. This retraining is natural and reasonable in terms of VQNHE training, as in the real problem, we can only train the neural network based on measurement results anyway. From another perspective, if retraining on the post-processing module can further lower the energy estimation, such post-processing is similar to a quantum error mitigation (QEM) workflow. VQNHE might have QEM baked in by adjusting the post-processing to alleviate the effect of quantum noise in the PQC. For the noisy simulator, we again collect 100 groups of measurements (8192 shots each group) to determine the mean value and standard deviation of energy estimation. The result pairs before and after neural network retraining are $(-5.858, 0.0290)$ and $(-5.867, 0.0246)$. In terms of hardware experiments, we collect bitstring on each required basis in 10 groups (8192 shots each group), and we compute the mean and standard deviation from a list of groups that are randomly selected by combining measurement groups on each basis. The result pairs before and after neural network retraining are $(-5.852, 0.0283)$ and $(-5.894, 0.0306)$. The results after retraining are reported in FIG.2 in the main text as the results of the noisy simulator and hardware. As we can see, the energy estimation is indeed

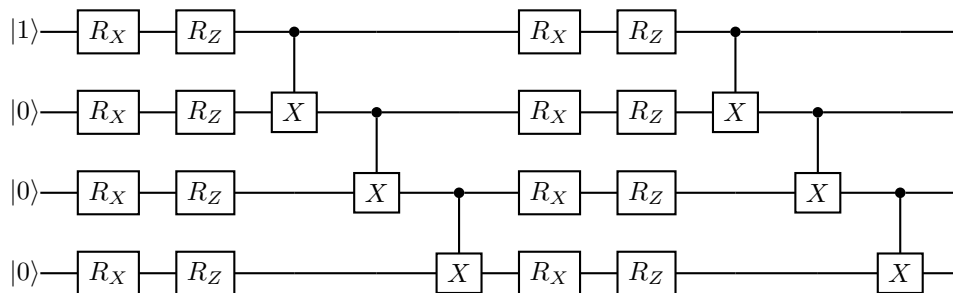


FIG. S3. Depth 2 hardware efficient ansatz utilized for VQNHE and VQE optimization on LiH. The input initial state is $|1000\rangle$ so that when the state goes through two rounds of CNOT gates, the output state is approximately $|1010\rangle$ when all rotational angles are small. Such state is the Hartree-Fock mean field solution under our symmetric binary qubit encoding.

lower with network retraining. In some sense, the observation indicates that quantum error is partially reduced by post-processing retraining. Since the energy gain after neural network retraining is larger in the real hardware case, retraining technique is more useful to suppress quantum error induced by real hardware which is not fully reproduced by noisy simulators.

Some further observations and comments are in order. The results from the noisy simulator and the real quantum hardware match well in both VQE and VQNHE cases. The standard deviation that characterizes the measurement uncertainty is similar in both cases. VQNHE has measurement uncertainty in the same order as VQE. This fact implies that the required number of measurement shots to reach a given accuracy is similar for VQNHE and VQE. Variational post-processing is potentially good for QEM but the error mitigation capacity is still limited since the energy gain brought by retraining is not enough to recover the ideal result. It deserves further investigation on the interplay between VQNHE and QEM.

Technical details for the simulation of LiH

The Hamiltonian of molecules can be described by the many-electrons' Schrödinger equation with Born-Oppenheimer approximation. In typical quantum chemistry setups, we first solve the equation with the Hartree-Fock approximation, where the ground state is assumed to be a single Slater determinant. The Hartree-Fock solution gives the so-called molecular orbitals which is the linear combination of atomic orbitals. We then use these molecular orbitals as the basis functions and transform the Schrödinger equation into the second quantization form. At this stage, the coefficients in the Hamiltonian are determined by the overlap integral between molecular orbitals. These values are calculated via Psi4 and OpenFermion-Psi4 plugin. Since we use the standard STO-3G atomic orbitals, there are $(1 + 5) * 2 = 12$ spin orbitals (independent fermions) in total. We further invoke the idea of the complete active space to restrict the freedoms. For the core orbitals 1s of Li, we assume they are always filled. And since the Li-H bond is mainly formed by the hybridization of H(1s) and Li(2s, 2pz), we regard Li(2px, 2py) as virtual orbitals that are never filled. Confining to the complete active space, we are left with only six fermionic degrees of freedom. After building the fermionic Hamiltonian, we further encode the Hamiltonian into qubits. There are many well-established encoding schemes such as Jordan-Wigner and Bravyi-Kitaev transformation. However, in our case, there are two conserved quantities, i.e., there are always an odd number of electrons in the spin up and spin down orbitals, we choose to further reduce the Hamiltonian to a 4-qubit representation using a parity conserved binary encoding provided by OpenFermion (See details for binary codes usage in https://quantumai.google/openfermion/tutorials/binary_code_transforms). The target Hamiltonian contains 100 terms of Pauli strings, and the coefficients before these Pauli strings may change as functions of bond distances.

Next, We optimize the target Hamiltonian energy with VQE and VQNHE. Both methods utilize the PQC as shown in Fig. S3. The parameters θ are initialized near zero, so that the output state from this PQC is in the form $|1010\rangle$, which is the Hartree-Fock solution (two electrons filled in the lowest molecule orbitals within the complete active space) under the binary encoding used in this case. With such an initialization trick and $|1000\rangle$ as the input state, VQE and VQNHE give stable performance and somehow avoid the issue of barren plateaus, since HF solution is generally a very good approximation for such small molecules. Besides, for the VQNHE case, the post-processing model is a lightweight fully connected neural network with two hidden layers of units 8 and ReLU activation. The

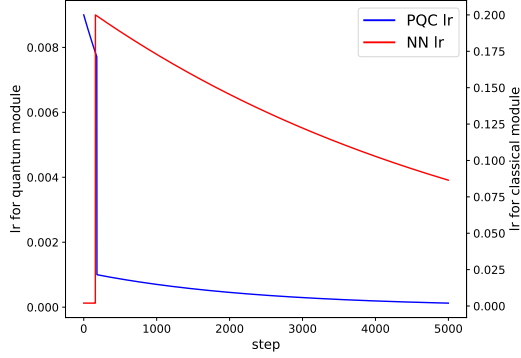


FIG. S4. The learning rates of both Adam optimizers for the PQC and neural network (NN) with different update steps in LiH energy optimization. Quantum spin model optimization shares similar learning curves though with slightly different value.

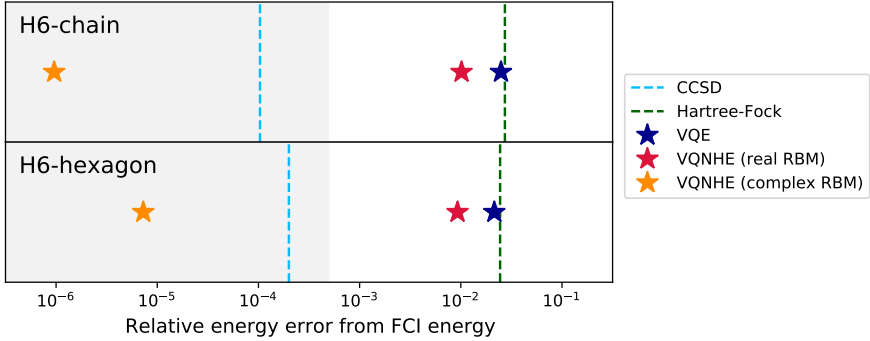


FIG. S5. Relative energy errors in H_6 -chain and H_6 -hexagon system. Energies obtained by Hartree-Fock method, CCSD method, VQE method, VQNHE method with both real and complex RBM post-processing are shown. The baselines for the relative error are obtained by FCI method. The gray shaded areas are within chemical accuracy. VQNHE with complex RBM post-processing even outperforms CCSD method.

final scalar output is activated by $e^{\phi_0 \tanh(*)}$, where ϕ_0 is a trainable weight for f and can be restricted in the norm to avoid large measurement fluctuations as we mentioned in the section above. We run $10 \sim 30$ VQE and VQNHE simulations (with different initializations) for each bond distance, and keep the lowest energy as the final converged energy value. In addition, we utilized the idea of adiabatic VQE, where the initialization from the best result in the last round is perturbed and serves as the initialization for the next Hamiltonian parameter when the bond distance is updated from the last round. This trick boosts the convergence of overall VQE training.

More on hyperparameters in VQNHE for LiH. Default initialization for parameters in the hardware efficient ansatz is drawn from a Gaussian distribution with a standard deviation of 0.2. We also perform initialization from the best initialization of the last and the second last sets of parameters by perturbation with a uniform noise with width 0.1. The cutoff for ϕ_0 is set to be 5 with an initial value of 1 while, in practice, the converged result often shows much smaller ϕ_0 indicating smaller fluctuations with measurement outcomes. The energy convergence threshold is set at 10^{-9} , Adam optimizers are utilized. The learning curves for both quantum and classical modules are shown in Fig. S4.

Technical details for the simulation of H_6 -hexagon and H_6 -chain

We follow similar procedures as in the case of LiH simulation to obtain the qubit Hamiltonian for both H_6 -hexagon and H_6 -chain molecules. The bond distances are fixed at 0.99 Å and 0.93 Å, respectively, as these distances should correspond to the equilibrium configurations for these systems. There are 12 spin orbitals for each molecule if the STO-3G basis set is used. Since the systems are not spin polarized, with the symmetry enforced qubit encoding, we can translate the electronic Hamiltonian to a qubit Hamiltonian using only 10 qubits. Namely, we save one qubit for each spin-up and spin-down subspaces for electrons.

The PQC utilized in both VQE and VQNHE is depth-4 hardware efficient ansatz, consisting of circuit layers that each is composed of Rx layer, Rz layer and CNOT layer. The initial state is given by $|1110100101\rangle$, which is transformed into the Hartree-Fock solution $|1110011100\rangle$ after 4 layers of CNOT gates. Therefore, with such an initial state and small initialization around zero for all rotation gates, the PQC can more easily converge to good approximations. As for the classical neural network part for the hybrid representation, we consider both real and complex RBM. The RBM neural architecture is given by:

$$f(\mathbf{s}) = e^{\sum_i a_i s_i} \prod_{j=1}^M 2 \cosh(b_j + \sum_i W_{ij} s_i), \quad (\text{S18})$$

where trainable parameters $\phi = \{W, a, b\}$. If these parameters are allowed to be complex numbers, we call the module complex RBM. The expressive power of the RBM is determined by the ratio between hidden units and visible units M/N . In our setup, $N = 10$ and $M = 40$. It is worth noting that this is the only part where we use complex post-processing modules throughout this work. The reason is that the phase structure of the ground state for such complex systems is hard to capture by the shallow circuit, and a more powerful classical post-processing module may share the burden with a shallow PQC. As clearly implied by the way this hybrid representation of quantum states is setup, as quantum hardware improves we may rely more on the expressive power of a deeper quantum circuit and refrain from using more sophisticated neural networks on the classical end.

We run the simulation using an ideal simulator, where more than 700 terms of Pauli strings in the Hamiltonian are compiled as one big matrix and its expectation value is optimized. Such Hamiltonian compiling technique can greatly reduce the required simulation time and resources. The results for both H_6 systems are shown in Fig. S5. The relative energy error is defined as $|(E - E_{\text{FCI}})/E_{\text{FCI}}|$. The results obtained with complex RBM post-processing are impressive as they are even much better than the values obtained from CCSD, which is known as the golden standard in quantum chemistry.

More on hyperparameters for VQNHE training on the H_6 system. Complex RBM is initialized with all weights around zero with a standard deviation 0.005. Parameters in the hardware efficient PQC are initialized around zero with a standard deviation 0.03. Both optimizers for the PQC and the RBM are Adam. The quantum part is mainly optimized in the first 200 rounds with the learning rate 0.01 and after 200 rounds, the learning rate for the i -th round reads $0.002 * 0.5^{(i-200)/800}$. The learning rate for updating the RBM is $0.006 * 0.5^{(i-200)/20000}$ after 200 rounds and 0.0006 for the first 200 optimization rounds.

Lastly, we comment that the energy optimization curve in the VQNHE case is very special. The optimization can make no progress for thousands of rounds and, suddenly, the energy will start to decrease again. Therefore, one needs very strict convergence criteria and must be patient during the optimization.
